

Supporting Information

Adsorption of Gaseous Mercury for Engineering Optimization: From Macrodynamics to Adsorption Kinetics and Thermodynamics

Qinyuan Hong^a, Haomiao Xu^{a,b,*}, Jiaxing Li^a, Lu Tong^a, Zhenxuan Tang^a,
Yuanxiang Xu^a, Wenjun Huang^a, Zan Qu^{a,b} and Naiqiang Yan^{a,b}

- a. School of Environmental Science and Engineering, Shanghai Jiao Tong University,
Shanghai 200240, China*
- b. Shanghai Institute of Pollution Control and Ecological Security, Shanghai
200092, China*

Number of Tables: 3

Number of Figures: 9

* Corresponding author; Tel: +86 21 54745591; Fax: +86 21 54745591
E-mail address: xuhaomiao@sjtu.edu.cn (Haomiao Xu).

List of Tables:

Table S1. Element composition analysis of CuS/Al₂O₃ measured by XRF.

Table S2. Experimental parameters of fixed-bed adsorption for bed length optimization

Table S3. Surface elements valences of fresh and spent CuS/Al₂O₃.

List of Figures:

Figure S1. XRD pattern of as-prepared CuS₍₁₋₂₎/Al₂O₃.

Figure S2. Sectional views of different CuS/Al₂O₃: (a) 0.5-1mm, (b) 1-2 mm, (c) 2-3 mm, and (d) 3-5 mm.

Figure S3. The Hg⁰ adsorption performance of 1-2 mm Al₂O₃.

Figure S4. The long-term effect of gas components on mercury adsorption performance over CuS/Al₂O₃: (a) O₂+SO₂ and (b) O₂+SO₂+H₂O.

Figure S5. Linear regression by fitting the data with Freundlich adsorption model.

Figure S6. The mercury adsorption breakthrough curves under different temperature.

Figure S7. Hg⁰-TPD experiment of spent CuS/Al₂O₃.

Figure S8. XPS spectra of fresh and spent CuS/Al₂O₃: (a) S 2p, (b) Cu 2p, and (c) Hg 4f.

Figure S9. The mercury adsorption performance of CuS/Al₂O₃ after Hg⁰-TPD experiment (without activation).

Table S1. Element composition analysis of CuS/Al₂O₃ measured by XRF.

Sorbents	Al (%)	Cu (%)	S (%)	CuS (%)
CuS _(0.5-1) /Al ₂ O ₃	18.74%	5.37%	3.87%	9.23%
CuS ₍₁₋₂₎ /Al ₂ O ₃	21.42%	3.21%	2.33%	5.53%
CuS ₍₂₋₃₎ /Al ₂ O ₃	19.69%	3.11%	1.98%	5.09%
CuS ₍₃₋₅₎ /Al ₂ O ₃	17.45%	1.70%	1.21%	2.92%

Table S2. Experimental parameters of fixed-bed adsorption for bed length optimization.

$[\text{Hg}^0]_{\text{in}}$ ($\mu\text{g m}^{-3}$)	f (mL min^{-1})	L_e (mm)	q_e ($\mu\text{g g}^{-1}$)	ρ (g cm^{-3})	D (mm)	t_b (min)	t_s (min)
1200	500	12	359	0.7958	20	400	1400

Table S3. Surface elements valences of fresh and spent CuS/Al₂O₃.

Sorbent	S ²⁻	S ¹⁻	SO ₄ ²⁻	Cu ⁺	Cu ²⁺	Hg ⁰	Hg ²⁺
Fresh	21.80%	10.85%	67.34%	49.37%	50.63%	-	-
Spent	22.67%	6.95%	70.38%	58.43%	41.57%	14.63%	85.37%

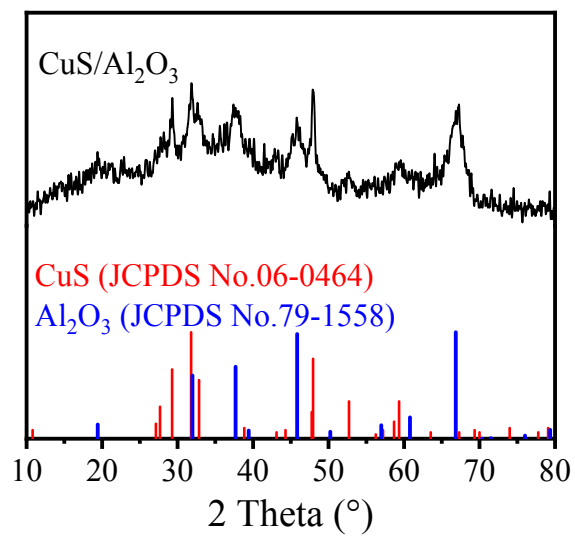


Figure S1. XRD pattern of as-prepared $\text{CuS}_{(1-2)}/\text{Al}_2\text{O}_3$.



Figure S2. Sectional views of different CuS/Al₂O₃: (a) 0.5-1mm, (b) 1-2 mm, (c) 2-3 mm, and (d) 3-5 mm.

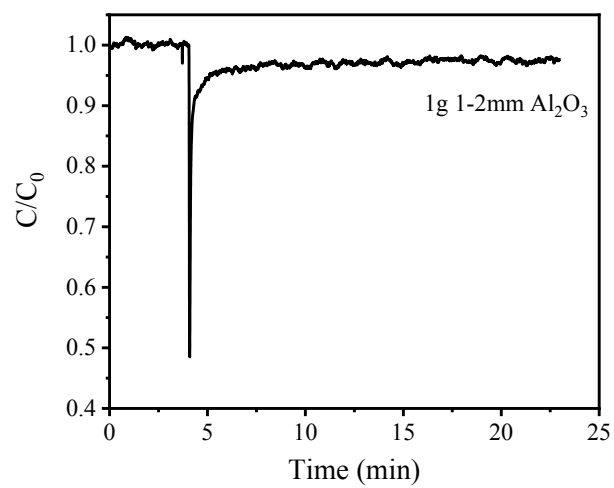


Figure S3. The Hg⁰ adsorption performance of 1-2 mm Al₂O₃.

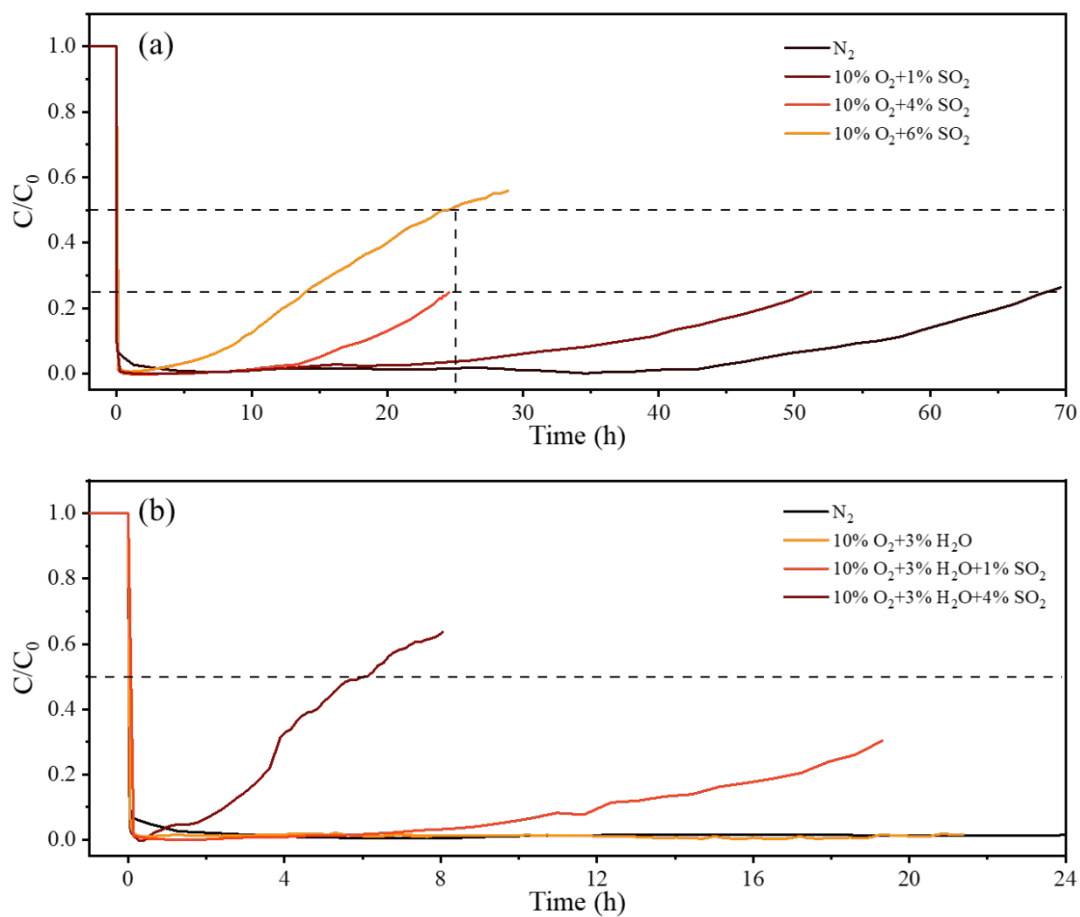


Figure S4. The long-term effect of gas components on mercury adsorption performance over CuS/Al₂O₃: (a) O₂+SO₂ and (b) O₂+SO₂+H₂O.

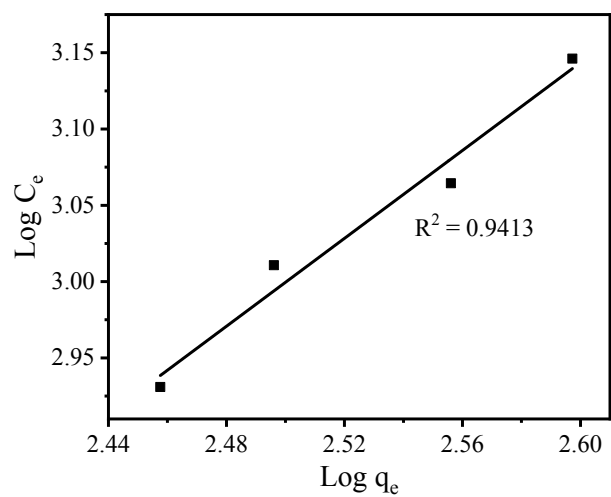


Figure S5. Linear regression by fitting the data with Freundlich adsorption model.

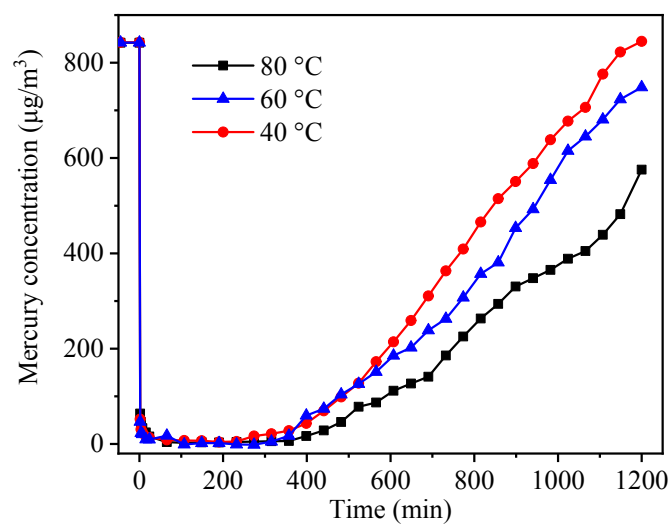


Figure S6. The mercury adsorption breakthrough curves under different temperature.

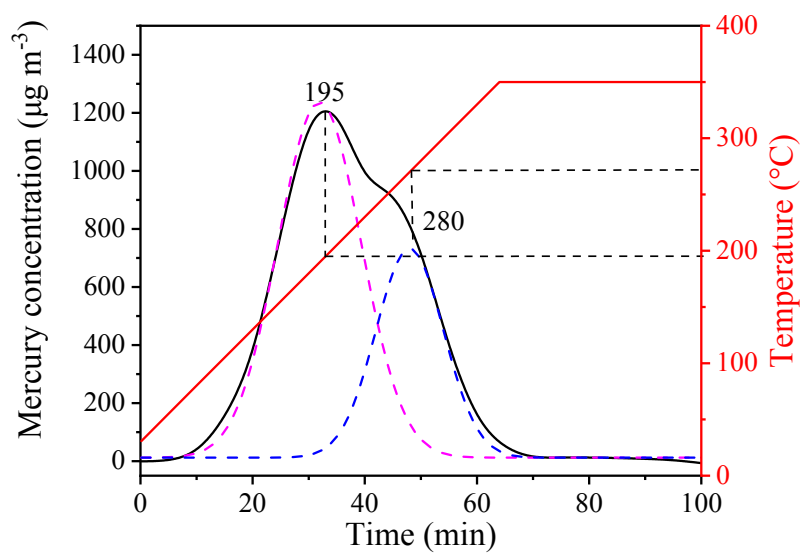


Figure S7. Hg^0 -TPD experiment of spent $\text{CuS}/\text{Al}_2\text{O}_3$.

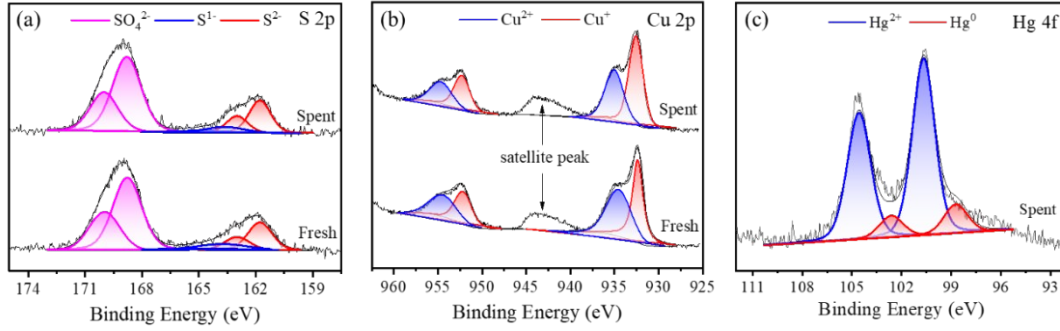
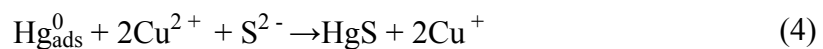
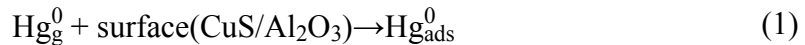


Figure S8. XPS spectra of fresh and spent CuS/Al₂O₃: (a) S 2p, (b) Cu 2p, and (c) Hg 4f.

Figure S7 illustrates the changes in the surface chemical valence of CuS/Al₂O₃ before and after mercury adsorption at 80 °C for 3h through XPS analysis. For S 2p in Figure 7Sa, the peaks located in 163.7 and 164.9 eV were assigned to S 2p_{3/2} and S 2p_{1/2} of S¹⁻, respectively, which were regarded as the active site for Hg⁰ adsorption in our previous works.¹ The peaks centered at 161.8 and 163.0 eV were attributed to S²⁻.² SO₄²⁻ featured its S 2p_{3/2} and S 2p_{1/2} spikes at 168.8 and 170.0 eV. For the results of Cu 2p, as shown in Figure 7Sb, the binding energies at 932.4 and 952.2 eV were consistent with the characteristics of Cu⁺, while those at 934.5 and 954.4 eV were ascribed to Cu²⁺ with the satellite peak at about 944 eV.³ After capturing Hg⁰, as list in Table S3, the proportion of S¹⁻ and Cu²⁺ in the spent CuS/Al₂O₃ decreased by 3.9% and 9.1%, respectively, while that of S²⁻ and Cu⁺ increased accordingly. Moreover, the spectrum in Hg 4f region included two forms of mercury. The fitting peaks located at 100.7 and 104.6 eV were attributed to Hg 4f_{7/2} and Hg 4f_{5/2} of Hg²⁺ (Figure 7Sc), owing to the formation of HgS.⁴ The peaks at 102.6 and 105.8 eV belonged to the spin-orbit doublet of the Hg⁰, which accounted for only 14.63% (Table S3). It indicated that the gaseous Hg⁰ was first physically adsorbed on CuS/Al₂O₃ surface (Hg⁰_{ads}), and then transferred to the chemisorption state (HgS), which could be described as following equations:



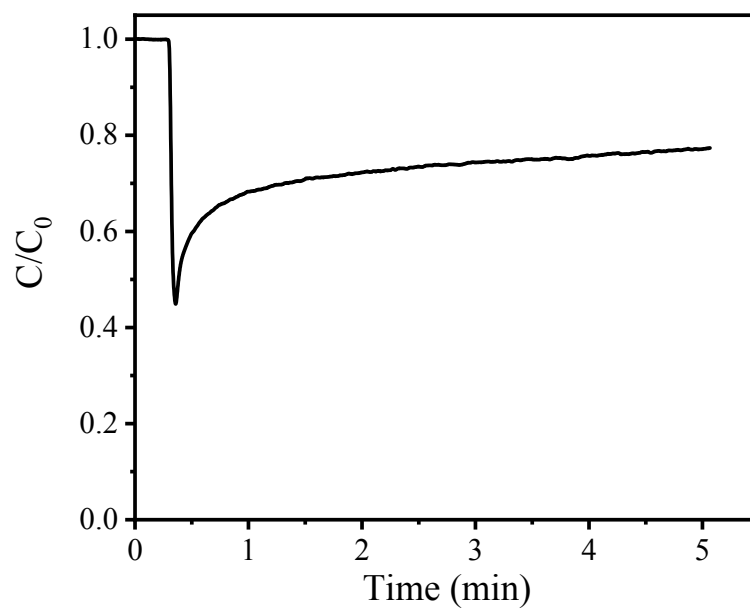


Figure S9. The mercury adsorption performance of CuS/Al₂O₃ after Hg⁰-TPD experiment (without activation).

1. Kartio, I. J.; Basilio, C. I.; Yoon, R. H., An XPS Study of Sphalerite Activation by Copper. *Langmuir* **1998**, *14*, (18), 5274-5278.
2. Smart, R. S. C.; Skinner, W. M.; Gerson, A. R., XPS of sulphide mineral surfaces: metal-deficient, polysulphides, defects and elemental sulphur. *Surf. Interface Anal.* **1999**, *28*, (1), 101-105.
3. Liu, P.; Huang, Y.; Yan, J.; Yang, Y.; Zhao, Y., Construction of CuS Nanoflakes Vertically Aligned on Magnetically Decorated Graphene and Their Enhanced Microwave Absorption Properties. *ACS Appl. Mater. Inter.* **2016**, *8*, (8), 5536-5546.
4. Quan, Z.; Huang, W.; Liao, Y.; Liu, W.; Xu, H.; Yan, N.; Qu, Z., Study on the regenerable sulfur-resistant sorbent for mercury removal from nonferrous metal smelting flue gas. *Fuel* **2019**, *241*, 451-458.
5. Ma, Y.; Mu, B.; Zhang, X.; Yuan, D.; Ma, C.; Xu, H.; Qu, Z.; Fang, S., Graphene enhanced Mn-Ce binary metal oxides for catalytic oxidation and adsorption of elemental mercury from coal-fired flue gas. *Chem. Eng. J.* **2019**, *358*, 1499-1506.